J. Fluid Mech. (1975), *vol.* 71, *part* 4, *pp.* 755–768
Printed in Great Britain

Horizontal momentum jets in rotating basins

By STUART B. SAVAGE
Department of Civil Engineering and Applied Mechanics,
McGill University, Montreal, Canada

AND RODNEY J. SOBEY
Sonderforschungsbereich 80, Karlsruhe University, Karlsruhe, Germany†

(Received 3 June 1974 and in revised form 18 April 1975)

In order to prevent stagnation and improve water quality, the intakes of many water-supply reservoirs have the form of momentum jets directed approximately radially into the storage. An analysis which idealizes this flow as consisting of a turbulent jet issuing horizontally from a circular orifice into a large rotating basin of deep water shows that the jet path is a spiral whose length scale L depends upon the rate of rotation and the kinematic momentum of the jet. Good agreement is found with flow-visualization experiments when the basin depth h is 'large' ($h/L \gtrsim 0{\cdot}21$). For small depths ($h/L \lesssim 0{\cdot}024$) the flow tends to be two-dimensional and the jet path is found to be straight. Full-scale reservoirs are usually shallow enough that the effect of the earth's rotation on the jet path is likely to be small. However these reservoirs are not inordinately shallow and tests with distorted hydraulic models are likely to show significant effects of rotation and can be misleading to the unsuspecting.

1. Introduction

In a pioneering investigation carried out at Imperial College for London's Metropolitan Water Board, White, Harris & Cooley (1955) studied means of controlling thermal stratification and stagnation in large reservoirs during calm weather. (Most of this work has been presented only in a private report to the client, but a portion has been described by Cooley & Harris 1954.) They proposed that the incoming water be concentrated into turbulent jets, whose momentum and entrainment would break up the stratification and mix and circulate the general body of water; most of London's storage reservoirs constructed in recent decades have employed this concept. Suspecting that the earth's rotation might influence the jet-forced flow pattern, White *et al.* (1955) undertook some comparative experiments with a $\frac{1}{2500}$ scale model of the existing Queen Mary Reservoir, London. The results of these flow-visualization experiments are reproduced in figure 1 (plate 1). In both cases the water in the model reservoir was initially stationary with respect to the basin and photographs were taken of the dyed

† Present address: Department of Engineering, James Cook University, Townsville 4811, Australia.

inlet water at the same three consecutive times after the initial efflux. The model reservoir is shown on the left-hand side of figure 1 without rotation and on the right-hand side with rotation. The effects of rotation on the flow fields are quite evident.

The present study is part of a general investigation at Imperial College into circulation and mixing characteristics in water-supply reservoirs. In this preliminary study of the effects of rotation on reservoir flow fields several of the complicating features present in an actual reservoir, such as wind forcing, density stratification and effects of boundaries and topography, have been omitted. The idealized problem to be discussed concerns the flow fields generated by momentum jets directed horizontally into a large basin containing water of the same density which is rotating with a constant angular velocity Ω about a vertical axis. The effect of rotation on the paths of the jets is the principal subject of study.

The paper begins with an analysis of a 'two-dimensional' laminar jet emerging from a vertical slit. Although this case is of little practical interest it provides a theoretical framework for the consideration of turbulent jets. The path of a turbulent jet originating from a circular orifice in 'deep water' is then predicted theoretically. The term 'deep water' is subsequently defined in terms of a length scale which depends upon the initial jet momentum and the rate of rotation of the basin. The predicted jet paths are compared with the results of flow-visualization experiments. The paper concludes with a short discussion of shallow-water effects.

2. Theoretical considerations

Laminar jet emerging from a vertical slit

In this section we mention briefly the results of an analysis (Savage & Sobey 1974) to determine the flow field, especially the path, of a laminar jet issuing from a vertical slit into a rotating basin of similar fluid. The flow field will be treated as essentially two-dimensional. From the work of Taylor (1917, 1921) and Proudman (1916) it is well known that a steady rotation of a two-dimensional flow system does not affect the velocity distribution (as long as the pressure does not enter the boundary conditions). It is immediately evident that the jet path is straight and the velocity field is the same as that which occurs when rotation is absent. However, it is useful to outline the analysis since it illustrates the physical balance established and also sets up a logical framework which can be employed to treat the case of a turbulent jet issuing from a circular orifice.

The flow is assumed to take place in water of finite depth contained in a basin semi-infinite ($\bar{x} > 0$) in horizontal extent having a horizontal plane bottom (see figure 2). The basin rotates with constant angular velocity Ω about the vertical ($\bar{z}$) axis. A thin jet emerges into the water (at rest with respect to the rotating frame) from a vertical slit contained in the vertical side wall ($\bar{x} = 0$) of the basin.

Here attention will be restricted to distances downstream of the jet orifice small in the sense that the integrated bed friction force arising from the jet is small compared with the initial jet momentum. The effects of bed friction will be neglected and changes in the surface elevation assumed to be small compared

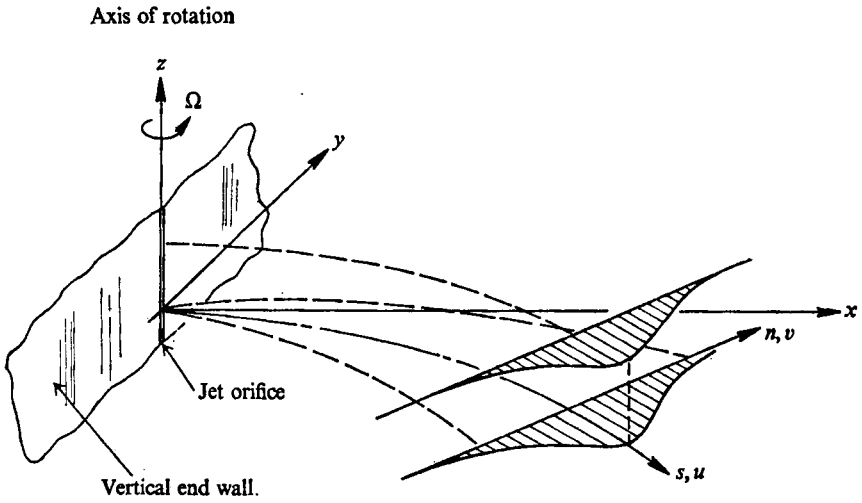

FIGURE 2. Definition sketch for plane laminar jet in rotating basin.

with the water depth. The flow field developed by the jet is therefore approximately two-dimensional.

It is convenient to use an orthogonal curvilinear co-ordinate system in which $\bar{s}$ is measured along the jet path and $\bar{n}$ is in the horizontal plane and normal to the jet path (figure 2). The equations for the steady motion of an incompressible viscous fluid in this system rotating with a constant angular velocity Ω (Greenspan 1968; Rosenhead 1963) are

$$\partial\bar{u}/\partial\bar{s} + \partial(h\bar{v})/\partial\bar{n} = 0, \tag{1}$$

$$\bar{u}\frac{\partial\bar{u}}{\partial\bar{s}} + \bar{v}\frac{\partial}{\partial\bar{n}}(h\bar{u}) - 2h\bar{v}\Omega = -\frac{1}{\rho}\frac{\partial\bar{p}}{\partial\bar{s}} + \nu h\frac{\partial}{\partial\bar{n}}\left\{\frac{1}{h}\left[\frac{\partial}{\partial\bar{n}}(h\bar{u}) - \frac{\partial\bar{v}}{\partial\bar{s}}\right]\right\}, \tag{2}$$

$$\bar{u}\frac{\partial\bar{v}}{\partial\bar{s}} + h\bar{v}\frac{\partial\bar{v}}{\partial\bar{n}} + \bar{K}\bar{u}^2 + 2h\bar{u}\Omega = -\frac{h}{\rho}\frac{\partial\bar{p}}{\partial\bar{n}} - \nu\frac{\partial}{\partial\bar{s}}\left\{\frac{1}{h}\left[\frac{\partial}{\partial\bar{n}}(h\bar{u}) - \frac{\partial\bar{v}}{\partial\bar{s}}\right]\right\}, \tag{3}$$

$$h = 1 - \bar{n}\bar{K}(\bar{s}), \tag{4}$$

where $\bar{u}$ and $\bar{v}$ are the velocity components in the $\bar{s}$ and $\bar{n}$ directions respectively, ν is the kinematic viscosity, ρ is the density and $\bar{p}$ is the reduced pressure defined by

$$\bar{p} = \tilde{p} + \rho g\bar{z} - \tfrac{1}{2}\rho\Omega^2(\bar{x}^2 + \bar{y}^2),$$

in which $\tilde{p}$ is the fluid pressure and g is the gravitational acceleration. The curvature of the jet path $\bar{K}(\bar{s})$ is positive if $d^2\bar{y}/d\bar{x}^2$ is positive along the jet path.

The present problem involves higher-order boundary-layer theory (Van Dyke 1969) and can be treated systematically by the method of matched asymptotic expansions. In the jet or boundary layer the variables are non-dimensionalized as follows:

$$s = \bar{s}/L^*, \quad n = Re^{\frac{1}{2}}\bar{n}/L^*, \quad u = \bar{u}/U^*, \quad v = Re^{\frac{1}{2}}\bar{v}/U^*, \quad p = \bar{p}/\rho U^{*2}, \quad K = \bar{K}L^*, \tag{5}$$

where U^* and L^* are the characteristic velocity and length and the Reynolds number $Re = U^*L^*/\nu$. The dependent variables are expanded for large Re in powers of $Re^{-\frac{1}{2}}$, for example

$$u(s,n) = u_1(s,n) + Re^{-\frac{1}{2}}u_2(s,n) + \ldots . \tag{6}$$

Substituting (5), (6), etc., into (1)–(4) and equating coefficients of like powers of $Re^{-\frac{1}{2}}$ yields the classical boundary-layer equations

$$\partial u_1/\partial s + \partial v_1/\partial n = 0, \tag{7}$$

$$u_1\frac{\partial u_1}{\partial s} + v_1\frac{\partial u_1}{\partial n} = -\frac{\partial p_1}{\partial s} + \frac{\partial^2 u_1}{\partial n^2}, \tag{8}$$

$$\partial p_1/\partial n = 0 \tag{9}$$

and the second-order boundary-layer equations, the one arising from (3) being

$$-Ku_1^2 + u_1/Ro = -\partial p_2/\partial n, \tag{10}$$

where the Rossby number $Ro = U^*/2\Omega L^*$.

There is no first-order outer flow and thus in the first-order boundary-layer equations $p_1 = 0$ and the appropriate solution to (7) and (8) is the classical solution of Schlichting (1968, p. 170) for a two-dimensional incompressible free laminar jet, which may be expressed in terms of a first-order stream function ψ_1 as

$$\psi_1 = 2s^{\frac{1}{3}}\tanh\eta, \tag{11}$$

where

$$\eta = n/3s^{\frac{2}{3}}.$$

The second-order outer-flow variables in the curvilinear $\bar{s}$, $\bar{n}$ system are

$$S = \bar{s}/L^*, \quad N = \bar{n}/L^*, \quad U = Re^{\frac{1}{2}}\bar{u}/U^*, \quad V = Re^{\frac{1}{2}}\bar{v}/U^*, \quad P = Re^{\frac{1}{2}}\bar{p}/\rho U^{*2}. \tag{12}$$

The matching conditions are

$$\lim_{N\to 0\pm} V(S,N) = \lim_{n\to\pm\infty}(v_1 - n\,\partial v_1/\partial n) = \mp\tfrac{2}{3}S^{-\frac{2}{3}} \tag{13}$$

and

$$\lim_{n\to\pm\infty} p_2 = \lim_{N\to 0\pm} P. \tag{14}$$

Equation (13) states that the first-order inner flow induces a sink distribution along the S axis in the second-order outer flow.

Substituting (12) into (1)–(4) yields the geostrophic second-order outer-flow equations, which can be solved to yield the pressure field P. Using the matching condition (14) it is found that

$$\lim_{n\to\pm\infty} p_2(s,n) = (\mp 2/Ro)s^{\frac{1}{3}}. \tag{15}$$

Integrating (10) over n and rearranging yields the following first approximation to the curvature:

$$K(s) = \left(-\int_{-\infty}^{\infty}\frac{u_1}{Ro}dn - [p_2(s,\infty) - p_2(s,-\infty)]\right)\Big/\int_{-\infty}^{\infty}u_1^2\,dn. \tag{16}$$

Using the first-order boundary-layer solution (11) and equation (15) in (16) it is found that the first term in the numerator of the right-hand side of (16) is exactly balanced by the second term and hence the curvature is identically zero.

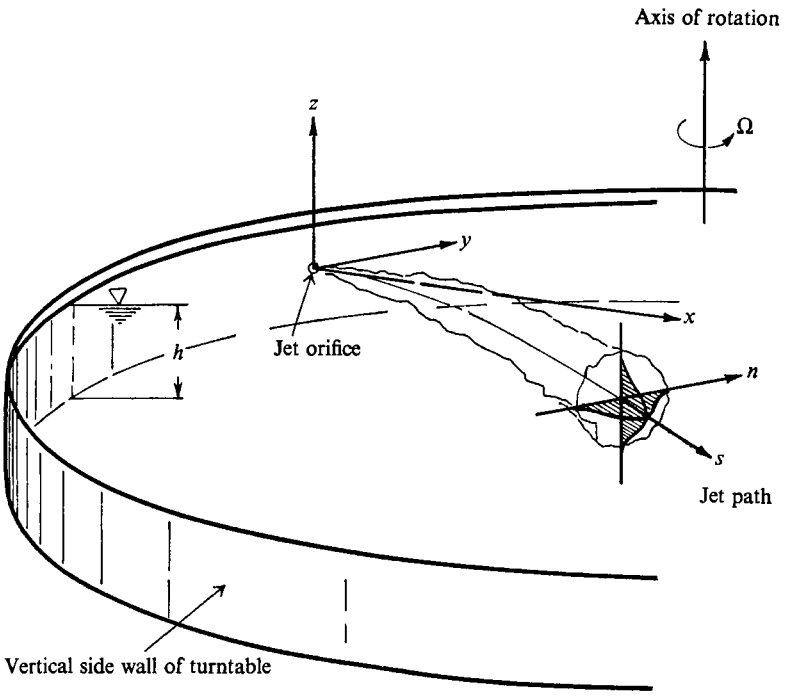

FIGURE 3. Definition sketch for round turbulent jet in rotating basin.

It is convenient to think of the situation physically in the following way. The first-order inner (jet) flow induces a second-order outer flow by entrainment. The geostrophic outer flow generates a pressure field which exactly balances the Coriolis acceleration of the inner (jet) flow and thus the jet path is straight. The pressure difference across the jet manifests itself as a change in the free-surface level across the jet. The jet acts rather like a vertical wall or barrier in supporting the pressure differences.

Turbulent jet emerging from circular orifice into deep water

The case in which a turbulent jet emanates horizontally from a circular orifice into a deep rotating basin of water (figure 3) can be treated in a manner directly analogous to the preceding analysis. In the previous 'two-dimensional' case, the dominant balance in the n direction was between the Coriolis acceleration and the pressure forces and such that the jet path was a straight line. The three-dimensional jet in the present case does not extend through the full depth of the water. In a very crude sense one may think of the jet as being unable to act as a barrier to support the pressure difference (between the two sides of the jet) necessary to straighten the jet path. One may determine the jet path in the spirit of the preceding two-dimensional laminar case using the ideas of higher-order boundary-layer theory. The present case involves an inner jet region where the flow is turbulent and a non-turbulent outer flow region. We cannot proceed in the mathematically logical and rigorous manner as in the previous case. For

example, the limit $Re \to \infty$ is not meaningful physically in the sense of the laminar jet. However, we can treat the turbulent jet in a corresponding way by separating the flow into inner and outer regions and progress in a rather heuristic fashion guided by the laminar analysis.

Consider the orthogonal curvilinear co-ordinate system $(\bar{s}, \bar{n}, \bar{z})$ shown in figure 3. The equations of motion (three-dimensional) may be expressed in a form analogous to (1)–(4). First let us determine the first-order 'inner' jet flow. Following the preceding analysis, to first order we neglect the effect of rotation and curvature on the jet development and take the mean axial velocity component $\bar{u}_s$ to be the same as that which would exist in the absence of rotation. To first order the pressure is constant. Empirically it is found that for a turbulent round jet $\bar{u}_s$ can be represented (cf. Schlichting 1968, p. 699; Newman 1967) as

$$\bar{u}_s = \frac{U^* L^*}{\bar{s}} \exp\left[-k\left(\frac{\bar{n}^2+\bar{z}^2}{l_0^2}\right)\right], \tag{17}$$

where $k = \ln 2$, U^* and L^* are characteristic velocity and length scales and $l_0 = \alpha \bar{s}$ is the jet half-width (i.e. the position where $\bar{u}_s$ is half the maximum centre-line velocity). The jet growth rate α is approximately 0·095 (Albertson *et al.* 1950; Newman 1967).

It is expedient at this stage to determine the component of velocity normal to the $\bar{s}$ axis at the 'edge' of the jet. It is convenient to use a cylindrical $(\bar{s}, \bar{r}, \theta)$ co-ordinate system (recalling that to first order the jet path is straight). Since the round-jet momentum flux

$$J_r = \rho \int_{-\infty}^{\infty} \int_{-\infty}^{\infty} \bar{u}_s^2 \, d\bar{z} \, d\bar{n}$$

is constant, (17) can be expressed as

$$\bar{u}_s = \frac{1}{\bar{s}\alpha}\left(\frac{2kJ_r}{\pi\rho}\right)^{\frac{1}{2}} \exp\left[-k\frac{\bar{r}^2}{\alpha^2\bar{s}^2}\right]. \tag{18}$$

Integrating the continuity equation

$$\frac{1}{\bar{r}}\frac{\partial}{\partial \bar{r}}(\bar{u}_r \bar{r}) + \frac{\partial \bar{u}_s}{\partial \bar{s}} = 0 \tag{19}$$

yields the normal velocity component at the 'edge' of the jet:

$$[\bar{u}_r]_{\bar{r}\to\infty} = -A/\bar{r}, \tag{20}$$

where

$$A = \alpha(J_r/2k\pi\rho)^{\frac{1}{2}}.$$

To second order the momentum equation in the $\bar{n}$ direction is the same as (10). Integrating this equation (expressed in terms of the physical variables) over $\bar{z}$ and $\bar{n}$ yields

$$\bar{K}(\bar{s}) \int_{-\infty}^{\infty} \int_{-\infty}^{\infty} \bar{u}_s^2 \, d\bar{z} \, d\bar{n} + 2\Omega \int_{-\infty}^{\infty} \int_{-\infty}^{\infty} \bar{u}_s \, d\bar{z} \, d\bar{n}$$

$$= -\left[\int_{-\infty}^{\infty} \bar{p}(\bar{s}, \infty, \bar{z}) \, d\bar{z} - \int_{-\infty}^{\infty} \bar{p}(\bar{s}, -\infty, \bar{z}) \, d\bar{z}\right], \tag{21}$$

which can be solved for the curvature $\bar{K}(\bar{s})$ of the jet path. The right-hand side of (21) represents the net pressure force in the $\bar{n}$ direction at the 'edges' of the jet. It can be determined by considering the second-order 'outer' flow (there is no first-order outer flow).

Imagine some limit process analogous to $Re \to \infty$ in the laminar case in which the inner jet flow shrinks to a curved line on the scale of the outer co-ordinates. Because of the first-order inner jet flow the second-order outer flow in effect is generated by a curved line sink, the geometry of which is as yet unknown. It is difficult to calculate the outer flow field due to the curved line sink and we shall merely determine the flow generated by a straight line sink. The approximation should be reasonable for distances from the sink axis which are small compared with the local radius of curvature of the sink (jet). The aim is to calculate the pressure field arising from the flow entrained by the jet. The second-order outer flow is inviscid but unlike the two-dimensional case the nonlinear convective terms are retained since the velocities are large near the sink. The equations of motion for the second-order outer flow expressed in a cylindrical co-ordinate system rotating with a constant angular velocity Ω are

$$\frac{1}{R}\frac{\partial}{\partial R}(RU_R)+\frac{1}{R}\frac{\partial U_\theta}{\partial \theta}+\frac{\partial U_S}{\partial S}=0, \tag{22}$$

$$U_R\frac{\partial U_R}{\partial R}+\frac{U_\theta}{R}\frac{\partial U_R}{\partial \theta}+U_S\frac{\partial U_R}{\partial S}-\frac{U_\theta^2}{R}-2\Omega U_S\cos\theta=-\frac{1}{\rho}\frac{\partial P}{\partial R}, \tag{23}$$

$$U_R\frac{\partial U_\theta}{\partial R}+\frac{U_\theta}{R}\frac{\partial U_\theta}{\partial \theta}+U_S\frac{\partial U_\theta}{\partial S}+\frac{U_RU_\theta}{R}-2\Omega U_S\sin\theta=-\frac{1}{\rho R}\frac{\partial P}{\partial \theta}, \tag{24}$$

$$U_R\frac{\partial U_S}{\partial R}+\frac{U_\theta}{R}\frac{\partial U_S}{\partial \theta}+U_S\frac{\partial U_S}{\partial S}+2\Omega(U_\theta\sin\theta-U_R\cos\theta)=-\frac{1}{\rho}\frac{\partial P}{\partial S}, \tag{25}$$

where U_R, U_S and U_θ are the physical (dimensional) velocity components in the R, S and θ directions and P is the pressure. The S axis, the axis of the jet (sink), is perpendicular to the axis of rotation. We seek a solution to (22)–(25) which behaves like a line sink for $R \to 0$. In analogy with (13) we have the matching condition

$$\lim_{R\to 0} U_R = \lim_{\bar{r}\to\infty} \bar{u}_r = -A/R, \tag{26}$$

making use of (20). The appropriate solution is found to be

$$U_R=-A/R-2\Omega S\cos\theta, \quad U_\theta=2\Omega S\sin\theta, \quad U_S=0, \tag{27)–(29}$$

$$P=-\rho A^2/2R^2-2\Omega\rho AS\cos\theta-2\Omega^2\rho S^2. \tag{30}$$

This flow corresponds to a sink flow ($U_R=-A/R$) plus a horizontal cross-flow which increases linearly with S. Figure 4 is a sketch of the outer-flow streamlines in the cross-flow plane.

The purpose of the analysis of the outer flow field is to determine the pressure field in order to evaluate the jet curvature $\bar{K}$ from (21). In analogy with (14) there is a matching condition

$$\lim_{\bar{r}\to\infty} \bar{p} = \lim_{R\to 0} P. \tag{31}$$

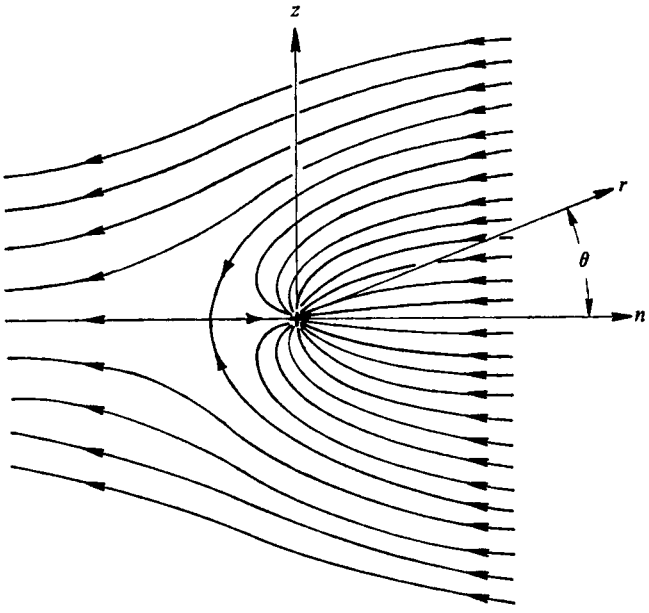

FIGURE 4. Outer-flow streamlines in cross-flow plane.

Thus in some overlap region

$$\bar{p}(\bar{s},\bar{n},\bar{z}) = P(R,S,\theta).$$

Then
$$\int_{-\infty}^{\infty} \bar{p}(\bar{s},\bar{n},\bar{z})\,d\bar{z} = \left\{ \begin{array}{ll} \displaystyle\int_{-\frac{1}{2}\pi}^{\frac{1}{2}\pi} PR\cos\theta\,d\theta & \text{for } \bar{n} \text{ positive,} \\ \displaystyle\int_{\frac{1}{2}\pi}^{-\frac{1}{2}\pi} PR\cos\theta\,d\theta & \text{for } \bar{n} \text{ negative.} \end{array} \right\} \tag{32}$$

By substituting (30) in (32) one can then obtain

$$\int_{-\infty}^{\infty} \bar{p}(\bar{s},\infty,\bar{z})\,d\bar{z} - \int_{-\infty}^{\infty} \bar{p}(\bar{s},-\infty,\bar{z})\,d\bar{z} = -2\rho A s\pi\Omega. \tag{33}$$

By using (18) and (33) in (21) one finally obtains for the jet curvature

$$\bar{K}(\bar{s}) = -\beta\bar{s}, \tag{34}$$

where
$$\beta = \alpha\Omega\left(\frac{2\pi}{k}\frac{\rho}{J_r}\right)^{\frac{1}{2}}.$$

Given the curvature of the jet as a function of $\bar{s}$, the path of the jet centre-line in the $\bar{x},\bar{y}$ plane can be determined. From the geometry of figure 5

$$d\delta/d\bar{s} = \bar{K}, \quad d\bar{x} = \cos\delta\,d\bar{s}, \quad d\bar{y} = \sin\delta\,d\bar{s}. \tag{35}$$

Equations (35) may be integrated to yield

$$\delta = -\tfrac{1}{2}\beta\bar{s}^2 \tag{36}$$

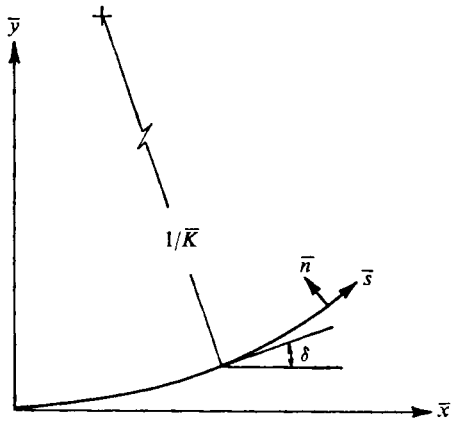

FIGURE 5. Definition sketch for jet path.

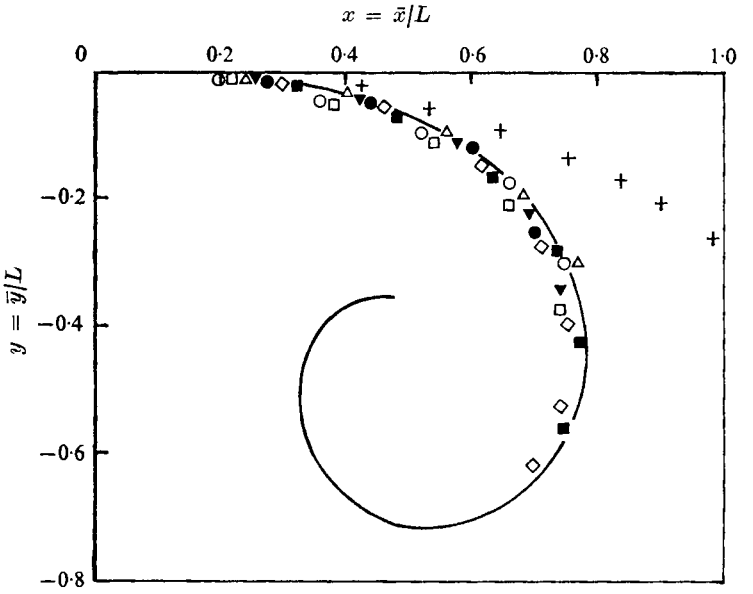

FIGURE 6. Theoretical jet path in deep water compared with turntable experiments. The symbols correspond to the following experiments: ○, *a*1; □, *a*2; △, *a*3; ▼, *a*4; ●, *b*2; ◇, *b*3; ■, *b*4; +, *c*2. ——, equations (37) and (38).

and the jet path may be expressed in parametric form as

$$x(t) = \frac{\bar{x}(t)}{L} = \int_0^t \cos\frac{\pi}{2}t^2\,dt = C(t), \tag{37}$$

$$y(t) = \frac{\bar{y}(t)}{L} = -\int_0^t \sin\frac{\pi}{2}t^2\,dt = -S(t), \tag{38}$$

where $t = (\beta/\pi)^{\frac{1}{2}}\bar{s}$, the natural length scale is

$$L = \left(\frac{\pi}{\beta}\right)^{\frac{1}{2}} = \left\{\frac{1}{\Omega\alpha}\left[\frac{\pi k}{2}\left(\frac{J_r}{\rho}\right)\right]^{\frac{1}{2}}\right\}^{\frac{1}{2}}, \tag{39}$$

and $C(t)$ and $S(t)$ are the Fresnel integrals (Abramowitz & Stegun 1965, p. 300). The predicted deep-water jet path is thus a clotoid (see figure 6), familiar from the Cornu spiral of wave diffraction theory. On physical grounds we might expect the analysis to be valid up to only a limited distance ($t \lesssim 1$) downstream of the orifice before the jet has become wrapped inside itself and interactions between different parts of the jet occur. One of the reviewers has pointed out that for the sake of self-consistency the analysis is restricted to downstream distances rather smaller than this. The analysis implies that the entrainment flow (altered by the Coriolis force) outside the jet region is small compared with the axial jet flow. The ratio of the outer cross-flow [equation (27)] to the axial centre-line velocity is $\pi(\bar{s}/L)^2$. Thus to be strictly correct the analysis is valid only for downstream distances such that $\pi(\bar{s}/L)^2$ is small. From (37) and (38) the maximum penetration predicted for the jet path (the maximum value of $C(t)$ at $t = 1{\cdot}0$) is $0{\cdot}78L$.

The spiral path of the jet may be explained simply by referring to (18) and (21). The jet curvature $\bar{K}(\bar{s})$ is seen to be proportional to the volume flux of the jet divided by its kinematic momentum flux. Since the volume flux increases with distance owing to entrainment while the momentum flux is constant to first order, the curvature $\bar{K}$ increases with $\bar{s}$ and the path is a spiral.

3. Experimental study

Flow-visualization experiments were conducted in the 5 m diameter rotating turntable facility in the Civil Engineering Hydraulics Laboratory at Imperial College, London. A detailed description of this facility is given by Sobey (1973). The turntable is based upon a large roller race on which is secured a rigid framework supporting an experimental basin. Rotation is by an electronic–hydraulic drive.

A 3·1 mm nylon-tube jet orifice was centrally positioned along a 1·5 m vertical wall that was aligned at right angles to the radius through the jet orifice. For all experiments the jet orifice was located at the mid-depth and was carefully aligned to issue at right angles to the vertical wall through a final 7·5 cm (25 diameters) length of straight tubing. The jet issued radially into a circular basin of diameter 5·04 m.

The jet discharge was provided by means of an air-pressured supply that was mounted on and rotated with the turntable. The discharge was measured by a Gallenkamp Gapmeter Lab-kit rotameter. The jet water was coloured with Process White, a water-based artist's paint. Special care was taken to ensure that the density and temperature of the dye solution and of the water in the turntable were the same, methyl alcohol being added to the dye solution where necessary. The discharge from the orifice was small in relation to the volume of water in the turntable and the residence times (initial basin volume/jet discharge, V_B/Q_0) were a minimum of 270 times the corresponding rotation periods $2\pi/\Omega$: no fluid was extracted from the rotating basin during the experiments.

A photographic tripod was constructed over and fixed to the rotating turntable. An automatic battery-powered Hasselblad 500 EL camera with a 50 mm Zeiss Distagon F4 wide-angle lens was mounted 6·0 m above the basin bed. Plan

Expt	h (cm)	Q_0 (cm^3/s)	$2\pi/\Omega$ (s)	$\frac{\Omega V_B}{2\pi Q_0}$	Re	J_r/ρ (cm^4/s^2)	L (cm)	h/L	L/D
$a1$	25	3·17	207·8	7380	1300	177	69·3	0·36	0·14
$a2$	25	5·08	206·8	4630	2090	455	87·8	0·28	0·17
$a3$	25	8·17	209·4	2870	3360	910	105·0	0·24	0·21
$a4$	25	10·4	211·7	2210	4280	1480	119·1	0·21	0·24
$b2$	25	4·67	102·5	10170	1920	385	59·2	0·42	0·12
$b3$	25	8·17	100·3	5930	3360	910	72·7	0·34	0·14
$b4$	25	11·3	101·2	4370	4660	1720	85·9	0·29	0·17
$c1$	2·5	6·91	251·6	271	2830	650	105·8	0·024	0·21
$c2$	7·5	5·75	233·6	1080	2360	452	93·1	0·081	0·18

TABLE 1. Experiments with turbulent round jets. Re based on average velocity and diameter of orifice. Velocity profile at orifice assumed to be parabolic for $Re < 2300$ and to follow a $\frac{1}{6}$-power law for $Re > 2300$ in calculation of J_r (Schlichting 1968, p. 560).

positioning within the rotating basin was facilitated by the delineation of a 20 cm square grid using a surveyor's chain and theodolite. This grid could be reconstructed for photographic purposes in the horizontal plane of the top of the basin wall (28 cm high) by stretching white cord between the appropriate points.

The water within the turntable was spun up to rigid-body rotation before the jet was discharged into the rotating basin. Approximately eight photographs of each jet flow were taken at suitable time intervals thereafter over approximately two revolutions of the turntable. The effect of the finite horizontal geometry of the basin should not be significant for such times; the relevant non-dimensional parameter (L/D, where L is the length scale defined by (39) and D is the basin diameter) had a maximum value of 0·24 for the experiments.

Flow rates Q_0 varied from 3·2 to 11·3 cm^3/s, rotation periods $2\pi/\Omega$ from 101 to 252 s and basin depths h from 2·5 to 25 cm. The full details of the experiments are given in table 1.

The photographic negatives were analysed by enlarging them with a Leitz projector to an appropriate scale defined by the length scale L computed from (39) and then tracing off the non-dimensional centre-line paths to a scale corresponding to figure 6. The definition of the path of the jet centre-line was a subjective process, but a reasonably consistent result was obtained by building up the jet path progressively through the eight or so exposures for each experiment.

Round turbulent jet in deep water

The series a and b experiments were undertaken to evaluate the above theoretical prediction of the path of the jet centre-line in 'deep water'. The water depth h was set as large as possible (25 cm) and only the jet discharge and the rotation period were varied. Figure 7 (plate 2) shows experiment $b3$ at various stages of development and is typical of both series of experiments.

Representative points from the observed paths for both series of experiments are shown, together with the theoretical prediction, in figure 6. The agreement is seen to be good, even beyond the point of maximum penetration. As mentioned

above, the present analysis is self-consistent only for $\pi(\bar{s}/L)^2$ small. The good agreement beyond the point of maximum penetration is to some extent fortuitous but at the same time typical of asymptotic analyses.

Round turbulent jet in shallow water

In very shallow water (of large horizontal extent), jet growth in the z direction would be restricted by both the bed and the free surface, no such severe restriction existing in the n direction. The jet would then become approximately two-dimensional and might support a larger pressure difference across its width (as does the plane laminar jet), which would tend to straighten the jet path. Alternatively, in very deep water (of large horizontal extent) the theoretical clotoid path should be valid for the initial development of the jet.

The relevant non-dimensional depth parameter is h/L, which has been evaluated for each experiment in table 1. This parameter varied from 0·21 to 0·42 for the series a and b experiments and the above results indicate that the lower value of 0·21 can be safely taken as a definition of 'deep water' in the present context. It is of course possible that this threshold value is even lower.

Two further experiments, $c1$ and $c2$ of table 1, were undertaken to obtain some preliminary clarification of the influence of shallow water. Figure 8 (plate 3) illustrates the shallow-water jet development of experiment $c1$ ($h/L = 0{\cdot}024$) at various times. For this experiment the natural length scale L was 105·8 cm, the maximum penetration of the 'deep water' jet path being $0{\cdot}78L = 82{\cdot}5$ cm, or about 4 of the grid squares in figure 8. Although there was some tendency towards a right-hand spiral path at small times (figures 8a–c) the path straightened out at larger times (figure 8f), implying that the jet was able to support a pressure difference across itself sufficient to balance the Coriolis accelerations. This conjecture is supported by a flow-visualization investigation (figure 9, plate 4) of the bottom boundary layer in this flow field using Process White, which undiluted is a heavy viscous slurry. The wall streamline orientations in the flow being entrained (the jet was only lightly coloured here) differed significantly across the jet, giving a clear indication that the pressure fields were different also.

For shallow water (small h/L) the bed friction strongly affects the overall jet development. Gadgil (1971) has studied laminar quasi-geostrophic jets and found that because of dissipation in the Ekman layers the jets cannot penetrate beyond a certain point. Although the jet initially entrains fluid near the exit, there is a station where the entrainment is zero, after which the jet ejects fluid. Prior to the maximum penetration there is a pronounced lateral spreading of the streamlines. Figure 8 [particularly (e) and (f)] seems to indicate this type of behaviour but it is difficult to obtain quantitative velocity-field data from flow visualization alone. One of us (R.J.S.) is at present conducting a detailed experimental study of the development of turbulent jets in shallow water and the results are forthcoming.

The remaining experiment ($c2$) was conducted at an intermediate relative depth hL of 0·081. Selected points from the observed path are shown in figure 6 together with points from the 'deep water' experiments and the theoretical

Reservoir	Capacity ($m^3 \times 10^6$)	Depth h (m)	'Diameter', D (km)	J_r/ρ (m^4/s^2)	L (km)	h/L	$\frac{0{\cdot}78L}{D}$
Queen Mary, 1925	30·6	11·6	1·8	6·4	0·70	0·017	0·30
Queen Elizabeth II, 1962	19·5	17·9	1·2	14·7	0·86	0·021	0·56
Wraysbury, 1972	34·5	20·4	1·5	95·6	1·36	0·015	0·71
Dachet, 1974	37·7	22·9	1·5	10·4	0·78	0·029	0·41

TABLE 2. Typical figures for London Metropolitan Water Board reservoirs. Latitude for all four reservoirs is 51·4° N, giving $2\Omega \sin \Phi = 1{\cdot}14 \times 10^{-4}$ rad/s.

clotoid path. It appears from the observed straightening of the jet path that this jet flow is able to support a pressure difference, but not one that is sufficient to balance the Coriolis accelerations.

4. Concluding remarks

The theoretical analysis of a turbulent jet issuing horizontally from a circular orifice into a large rotating basin of deep water predicts that the jet path is a clotoid which has a length scale

$$L = \left\{\frac{1}{\Omega\alpha}\left[\frac{\pi k}{2}\left(\frac{J_r}{\rho}\right)\right]^{\frac{1}{2}}\right\}^{\frac{1}{2}}.$$

The predicted path was found to agree closely with the experimentally measured paths when the non-dimensional depth was 'large' ($h/L \gtrsim 0{\cdot}21$). When the depth is 'small' ($h/L \lesssim 0{\cdot}024$) the confining effects of the upper free surface and the basin bed tend to make the mean flow two-dimensional. In this case rotation has little effect on the velocity field (see Taylor 1917, 1921; Proudman 1916) and the jet path is straight, as it would be in the absence of rotation.

These results are of considerable importance in connexion with hydraulic model tests to study the effects of various jet-inlet locations on the mixing and circulation patterns in water-supply reservoirs, for example the studies of White *et al.* (1955) mentioned previously (see figure 1). Typical parameters including $0{\cdot}78L/D$ and h/L for the prototype reservoirs of London's Metropolitan Water Board are given in table 2 (see also Sobey 1973). (In the determination of L, Ω in (39) has been replaced by $\Omega \sin \Phi$, where Φ is the latitude.) The values for h/L are all small and it is expected that the earth's rotation would have only a small effect on the jet paths and hence the overall circulation patterns. It should be noted however that the detailed structure of the slow-moving gyres or swirls on both sides of the jet and forced by it is dependent upon rotation (Sobey 1973). It is common practice in hydraulic modelling to distort the vertical and horizontal scales to ensure that the depths are large enough to produce turbulent flow throughout most of the model. If only moderate distortions were performed, say the vertical scales were increased by a factor of 5–10, then h/L for the model would be in the region where rotation would have an appreciable effect on the flow patterns and the model tests could be quite misleading. Some care is necessary

if proper hydraulic modelling is to be achieved and obviously relatively large rotating model basins are required if low Reynolds number effects are to be avoided in undistorted models. Further work is needed to investigate the cases where density differences exist between the inlet jet and the reservoir water.

The major part of this work was carried out in the Hydraulics Laboratory, Civil Engineering Department, Imperial College, London under the direction of Professor J. R. D. Francis. This paper was completed with the support of the Science Research Council (G.B.), the National Research Council of Canada and the Deutsche Forschungsgemeinshaft (through the Sonderforschungsbereich 80, Karlsruhe University).

REFERENCES

ABRAMOWITZ, M. & STEGUN, I. A. (eds) 1965 *Handbook of Mathematical Functions*, p. 300. Dover.

ALBERTSON, M. L., DAI, Y.B., JENSON, R. A. & ROUSE, H. 1950 *Trans. A.S.C.E.* **115**, 639.

COOLEY, P. & HARRIS, S. L. 1954 *J. Inst. Water Engng*, **8**, 517.

GADGIL, S. 1971 *J. Fluid Mech.* **47**, 417.

GREENSPAN, H. P. 1968 *The Theory of Rotating Fluids*. Cambridge University Press.

NEWMAN, B. G. 1967 In *Fluid Mechanics of Internal Flows* (ed. G. Sovran), p. 170. Elsevier.

PROUDMAN, J. 1916 *Proc. Roy. Soc.* A **92**, 408.

ROSENHEAD, L. (ed.) 1963 *Laminar Boundary Layers*. Oxford University Press.

SAVAGE, S. B. & SOBEY, R. J. 1974 Horizontal momentum jets in rotating basins. *Dept. Civil Engng Appl. Mech., McGill University Rep.* FML 74–1.

SCHLICHTING, H. 1968 *Boundary Layer Theory*. McGraw-Hill.

SOBEY, R. J. 1973 Ph.D. thesis, Civil Engineering Department, Imperial College, London.

TAYLOR, G. I. 1917 *Proc. Roy. Soc.* A **93**, 99.

TAYLOR, G. I. 1921 *Proc. Roy. Soc.* A **100**, 114.

VAN DYKE, M. 1969 *Ann. Rev. Fluid Mech.* **1**, 265.

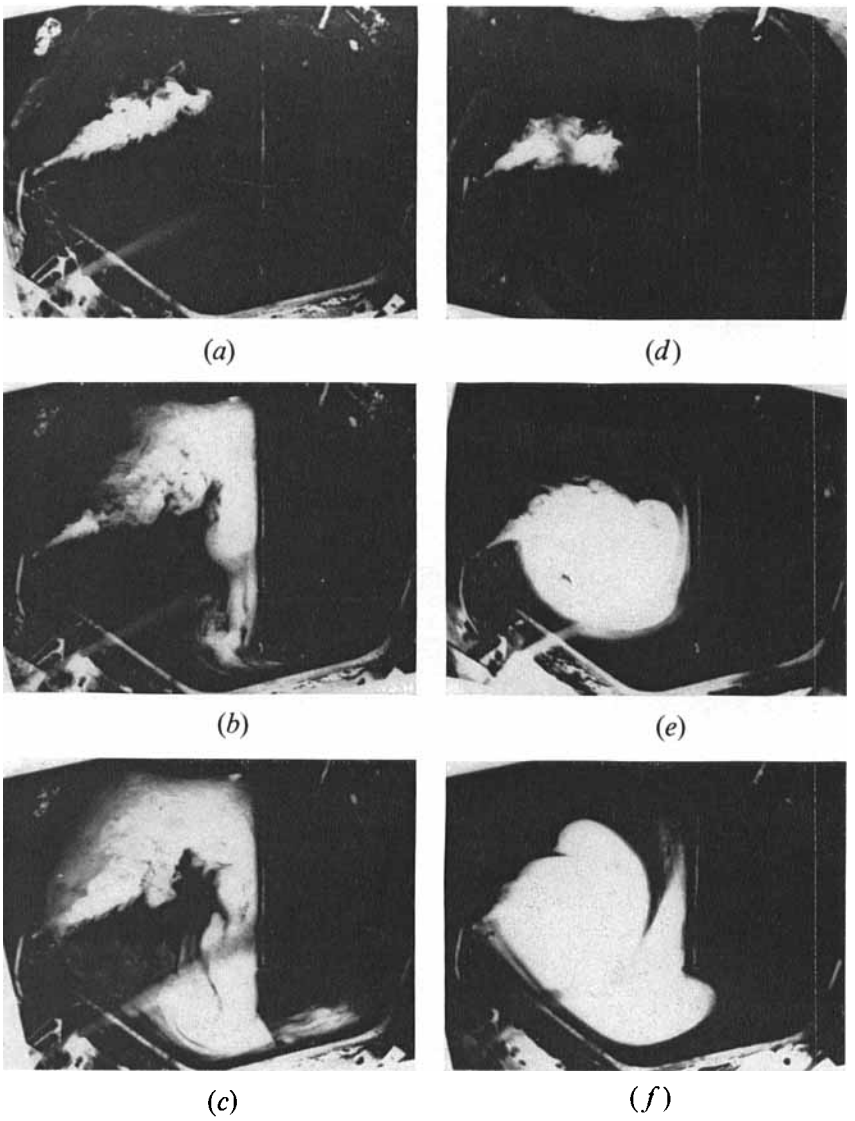

FIGURE 1. Flow in 1:2500 model of Queen Mary Reservoir. (*a*)–(*c*) show penetration of new water with model stationary after (*a*) $10\frac{1}{2}$, (*b*) $52\frac{1}{2}$ and (*c*) 105 h prototype. (*d*)–(*f*) show penetration of new water with model rotating, to study the effects of terrestrial rotation on the flow patterns, after (*d*) $10\frac{1}{2}$, (*e*) $52\frac{1}{2}$ and (*f*) 105 h prototype. (From White *et al.* 1955.)

(*Facing p.* 768)

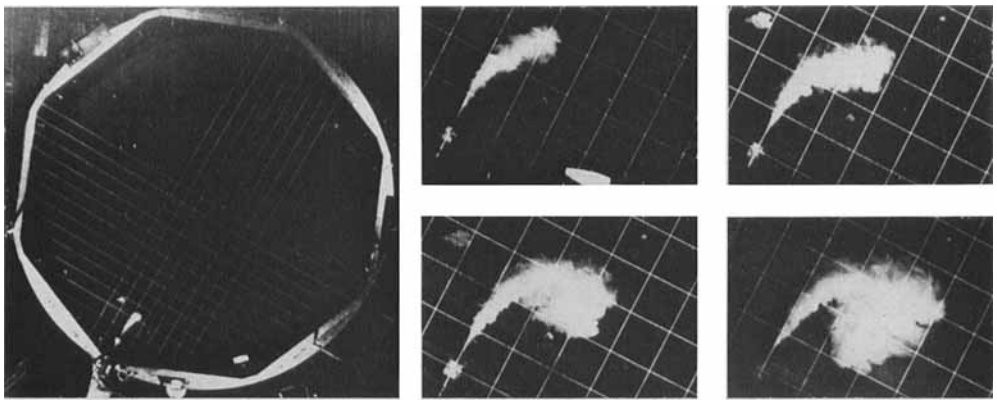

FIGURE 7. Development of jet in 'deep' water for experiment *b*3.

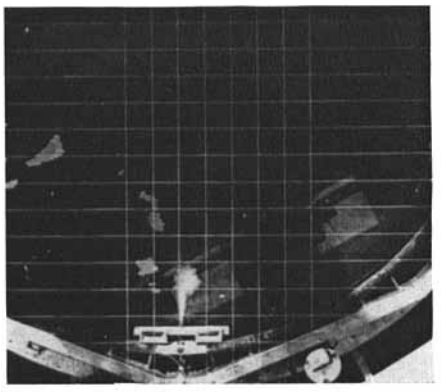

(*a*)

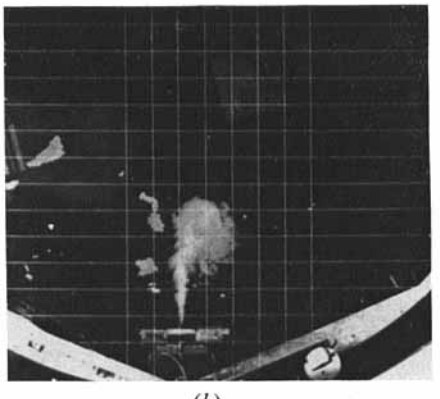

(*b*)

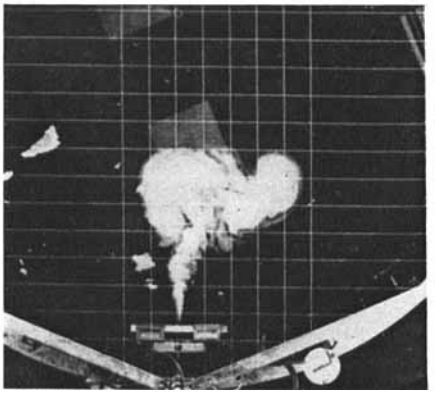

(*c*)

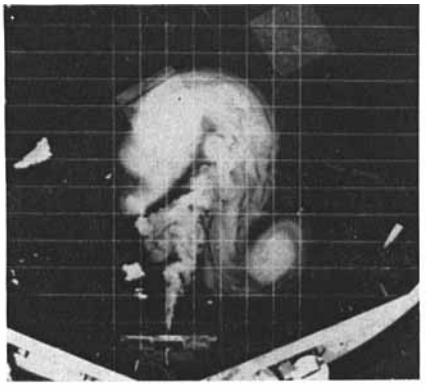

(*d*)

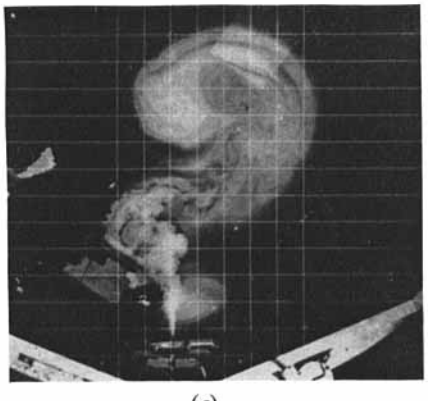

(*e*)

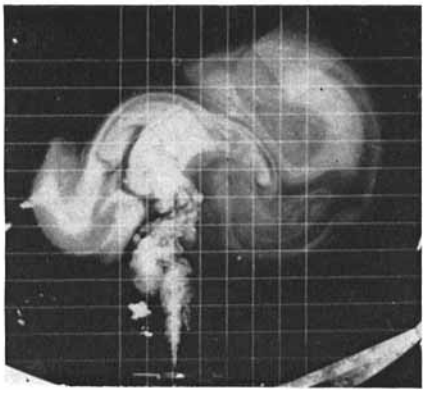

(*f*)

FIGURE 8. Development of jet in 'shallow' water for experiment *c*1.
(*a*)–(*f*) taken at increasing times from dye injection.

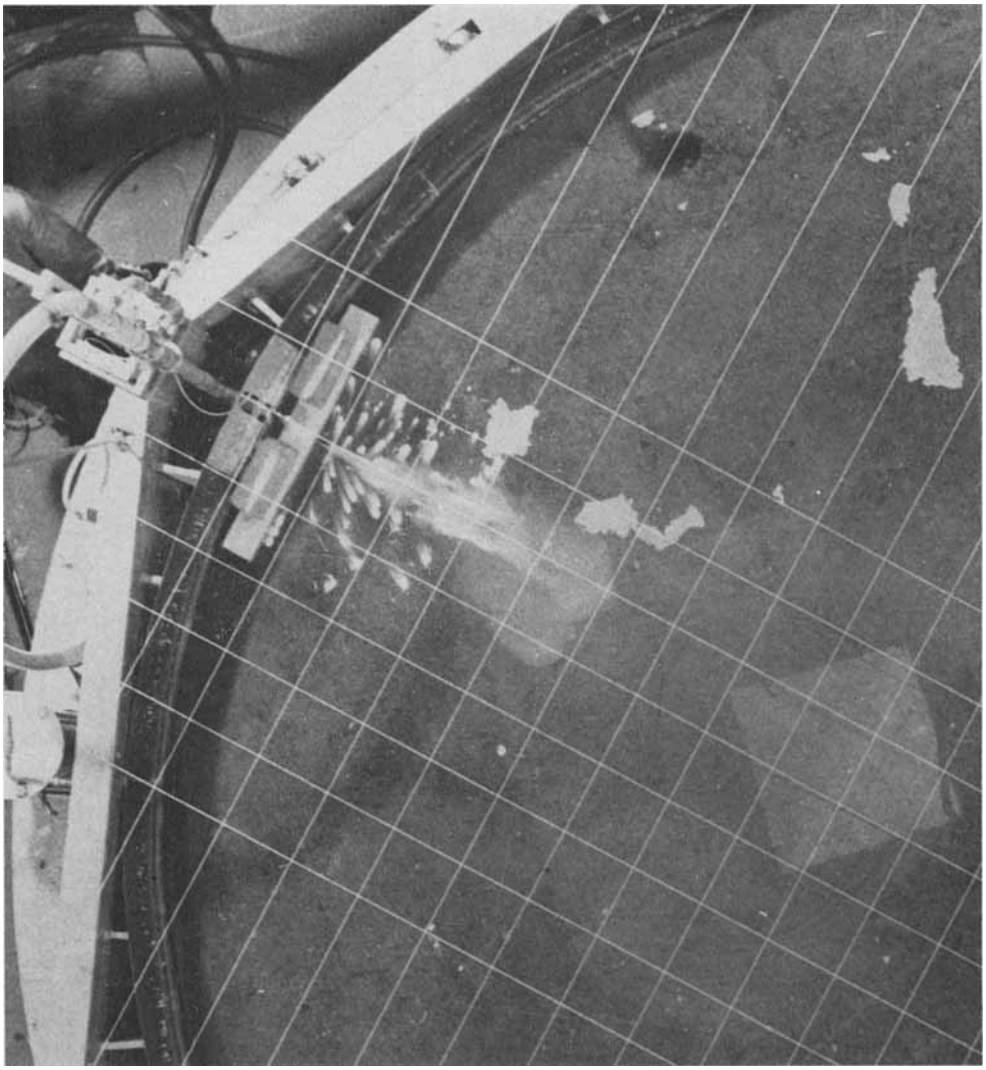

FIGURE 9. Streamlines in bottom boundary layer for experiment *c*1.